Molecules and Cells

SHORT-ROOT Controls Cell Elongation in the Etiolated Arabidopsis Hypocotyl

Souvik Dhar[1,2,4], Jinkwon Kim[1,4], Eun Kyung Yoon[1,3], Sejeong Jang[1], Kangseok Ko[1], and Jun Lim[1,*]

[1]Department of Systems Biotechnology, Konkuk University, Seoul 05029, Korea, [2]Present address: School of Biological Sciences, College of Natural Science, Seoul National University, Seoul 08826, Korea, [3]Present address: Department of Chemical and Biomolecular Engineering, National University of Singapore, Singapore 117585, Singapore, [4]These authors contributed equally to this work.
*Correspondence: jlim@konkuk.ac.kr
https://doi.org/10.14348/molcells.2021.5008
www.molcells.org

Transcriptional regulation, a core component of gene regulatory networks, plays a key role in controlling individual organism's growth and development. To understand how plants modulate cellular processes for growth and development, the identification and characterization of gene regulatory networks are of importance. The SHORT-ROOT (SHR) transcription factor is known for its role in cell divisions in Arabidopsis (*Arabidopsis thaliana*). However, whether SHR is involved in hypocotyl cell elongation remains unknown. Here, we reveal that SHR controls hypocotyl cell elongation via the transcriptional regulation of *XTH18*, *XTH22*, and *XTH24*, which encode cell wall remodeling enzymes called xyloglucan endotransglucosylase/hydrolases (XTHs). Interestingly, SHR activates transcription of the *XTH* genes, independently of its partner SCARECROW (SCR), which is different from the known mode of action. In addition, overexpression of the *XTH* genes can promote cell elongation in the etiolated hypocotyl. Moreover, confinement of SHR protein in the stele still induces cell elongation, despite the aberrant organization in the hypocotyl ground tissue. Therefore, it is likely that SHR-mediated growth is uncoupled from SHR-mediated radial patterning in the etiolated hypocotyl. Our findings also suggest that intertissue communication between stele and endodermis plays a role in coordinating hypocotyl cell elongation of the Arabidopsis seedling. Taken together, our study identifies SHR as a new crucial regulator that is necessary for cell elongation in the etiolated hypocotyl.

Keywords: GRAS, hypocotyl growth, SHORT-ROOT, transcriptional regulation, xyloglucan endotransglucosylase/hydrolase

INTRODUCTION

Despite their sessile nature, plants are remarkably flexible in their growth and development, enabling them to adapt to the ever-changing environmental conditions. In particular, hypocotyl growth, which is mainly controlled by cell elongation, is influenced by various environmental signals and intrinsic factors (Chaiwanon et al., 2016). To understand how environmental stimuli and developmental programs coordinately regulate cellular processes for plant growth and development, the hypocotyl of the reference plant Arabidopsis (*Arabidopsis thaliana*) has served as a reasonably attractive model system (Boron and Vissenberg, 2014; Chaiwanon et al., 2016).

In particular, the hypocotyl of dark-grown (etiolated or skotomorphogenic) Arabidopsis seedlings exhibits drastic cell elongation. For example, the epidermis cells in the etiolated Arabidopsis hypocotyl increase in length by approximately 100-fold, as compared with those in the embryo

Received 21 October, 2021; revised 22 November, 2021; accepted 1 December, 2021; published online 20 January, 2022

eISSN: 0219-1032

(Gendreau et al., 1997; Refrégier et al., 2004). It is widely believed that selective loosening and remodeling of cell walls by cell wall modifying enzymes play important roles in cell elongation (Chebli and Geitmann, 2017; Cosgrove, 2005; 2016a; 2016b). Indeed, previous work demonstrated that overexpression of genes which encode cell wall remodeling enzymes such as xyloglucan endotransglucosylase/hydrolases (XTHs) promoted hypocotyl cell elongation of etiolated Arabidopsis seedlings (Miedes et al., 2013). Nonetheless, the relationship between upstream transcription factors and downstream cell wall modifying enzymes (e.g., which transcription factors regulate which cell wall modifying enzymes for hypocotyl growth) requires further elucidation.

The SHORT-ROOT (SHR) transcription factor is a key regulator for formative and proliferative cell divisions in Arabidopsis roots and shoots (Benfey et al., 1993; Carlsbecker et al., 2010; Cruz-Ramírez et al., 2012; Dhondt et al., 2010; Helariutta et al., 2000; Levesque et al., 2006; Lucas et al., 2011; Sozzani et al., 2010). Both SHR protein and mRNA are localized in the stele, but the protein moves to the adjacent cells (e.g., endodermis, ground tissue stem cells, and quiescent center) to regulate expression of target genes, indicating that SHR acts as a mobile transcription factor (Cui et al., 2007; Gallagher and Benfey, 2009; Gallagher et al., 2004; Gardiner et al., 2011; Koizumi et al., 2012a; 2012b; Nakajima et al., 2001; Yoon et al., 2016). In the canonical mode of action, SHR acts in conjunction with its partner transcription factor, SCARECROW (SCR), to activate expression of downstream target genes (Carlsbecker et al., 2010; Cruz-Ramírez et al., 2012; Cui et al., 2007; Dhondt et al., 2010; Gallagher et al., 2004; Hirano et al., 2017; Koizumi et al., 2012a; 2012b; Nakajima et al., 2001; Sozzani et al., 2010; Yoon et al., 2016). In contrast to SHR localization, SCR localization is excluded from the stele (Di Laurenzio et al., 1996; Wysocka-Diller et al., 2000), thus indicating that the SCR-independent SHR pathway may also occur in the stele. However, this has yet to be verified.

Previous studies reported that as in the root of the *shr* seedling, the hypocotyl of the etiolated *shr* seedling did not possess functional endodermis in the ground tissue, resulting in no response to a change in the gravity vector (Fukaki et al., 1998; Kim et al., 2017; Morita et al., 2007; Yoon et al., 2016). In addition, the etiolated *shr* hypocotyl showed stunted growth (Fukaki et al., 1998; Yoon et al., 2016), implying that apart from its role in cell division, SHR may be involved in another growth parameter, cell elongation. However, the role of SHR in hypocotyl cell elongation is currently unknown.

In this study, we employed various experimental approaches, including phenotypic, transcriptomic, molecular, and genetic analyses, to unravel the role of SHR in cell elongation. Overall, we reveal that SHR is necessary for cell elongation in the etiolated Arabidopsis hypocotyl. Genome-wide transcriptome analyses allowed us to the identification of several *XTH* genes that were down-regulated in the etiolated *shr* hypocotyl. We found that SHR directly activated transcription of three of these differentially expressed *XTH* genes. Interestingly, unlike the known mode of action, transcriptional activation of these *XTH* genes was subject to the SCR-independent SHR regulation. Furthermore, we also found that confinement of SHR protein in the nuclei of the stele cells was able to promote cell elongation of the etiolated *shr* hypocotyl, despite the defective radial organization of the ground tissue. Taken together, our results provide novel and significant insights into the previously unknown regulatory role of SHR in the Arabidopsis hypocotyl.

MATERIALS AND METHODS

Plant material and growth conditions

In this study, we used the Columbia ecotype as the wild-type (WT) control. The mutants and the transgenic lines are as follows: *shr-2* (Benfey et al., 1993; Fukaki et al., 1998; Helariutta et al., 2000), *shr-6* (Yu et al., 2010), *scr-5* (Heo et al., 2011; Paquette and Benfey, 2005), *ProSHR::SHR-GFP* (Nakajima et al., 2001), *xth18-1* (SALK_025862), *xth22-2* (SAIL_158_A07), and *xth24-1* (SALK_005941C). We performed polymerase chain reaction (PCR)-based genotyping to verify homozygous plants from genetic crosses. Seeds were surface-sterilized, vernalized for 3 days at 4°C in the dark, and grown on half-strength of Murashige-Skoog (MS) agar plates (0.5X MS salt mixture, 0.5 mM MES, pH 5.7-5.8, 1% sucrose, and 1% agar) as described previously (Heo et al., 2011; Lee et al., 2016; Yoon et al., 2016). For phenotypic analysis of etiolated seedlings, seeds grown on 0.5X MS agar plates were treated with white light for 24 h, and subsequently transferred into the dark as described previously (Sun et al., 2016; Yoon et al., 2016). For genetic crosses and seed multiplication, seedlings grown on 0.5X MS agar plates were transferred to soil and grown under long day conditions (16-h light/8-h dark cycles) to maturity as described previously (Heo et al., 2011; Lee et al., 2016; Yoon et al., 2016). The sequence information of PCR primers used for genotyping is listed in Supplementary Table S1.

Hypocotyl phenotype analysis

For phenotypic analysis of the etiolated hypocotyls, the etiolated seedlings ($n > 30$ at each time point) were photographed with a digital camera (Olympus, Japan), and the hypocotyl length of each seedling was measured by using NIH Image J software (http://rsb.info.nih.gov/ij) as previously described (Oh et al., 2014; Sun et al., 2016). We independently repeated each experiment three times for biological replicates, and the data were analyzed using the Microsoft Excel program 2016 (Microsoft, USA). To analyze individual cell length in the hypocotyl, the etiolated seedlings were immersed in 70% ethanol overnight, and dehydrated through sequential ethanol series (80%, 90%, and 100% EtOH) for 30 min each. The samples were subsequently cleared with sodium hydroxide solution (7% NaOH in 60% EtOH) for 1 h, and sequentially exposed to a series of glycerol solutions (10% glycerol in 50% EtOH, 30% glycerol in 30% EtOH, and 0.01% TritonX-100 in 50% glycerol). The cleared etiolated seedlings ($n > 30$) were mounted on a glass slide with 0.01% TritonX-100 in 50% glycerol. Because both *shr* and *scr* mutants have no endodermis in the hypocotyl ground tissue (Fukaki et al., 1998; Yoon et al., 2016), the lengths of the inner cortex cells along the longitudinal axis of the hypocotyl were measured using an Axio Imager.A1 microscope

equipped with AxioCam MRc5 digital camera (Zeiss, Germany).

Transcriptomic analysis

For microarray and RNA-Seq experiments, total RNA samples were purified from 6-day-old etiolated WT and *shr-2* hypocotyls using RNeasy Plant Mini Kits (Qiagen, Germany) as described previously (Lee et al., 2016; Yoon et al., 2016). The microarray experiments were performed using Affymetrix ATH1 GeneChips (Affymetrix, USA) by DNA Link (DNA Link, Korea). The results from biological triplicates were normalized with Affymetrix Microarray Suite 5.0 (MAS 5.0), and the differentially expressed genes (DEGs) (> 1.5-fold and $P < 0.05$) were selected for further analysis. Raw data (CEL files) were deposited in the Gene Expression Omnibus (http://www.ncbi.nlm.nih.gov/geo/) (GEO accession No. GSE97670). RNA-Seq was conducted using Illumina HiSeq 2500 platform (Illumina, USA) by DNA Link (DNA Link). The paired-end reads (2X 100 bp length) generated by the Illumina HiSeq 2500 system were initially processed to remove the low-quality reads and adapter sequences (Bolger et al., 2014). Next, the high-quality reads for each sample were mapped to the Arabidopsis genome TAIR v10 by TopHat, and the alignment files generated by TopHat were used as input for Cufflinks (ver. 2.2.0). The DEGs (> 1.5-fold, $P < 0.05$ and FDR < 0.1) were identified by the Cuffdiff program by estimating FPKM (reads per kilobase of transcript per million mapped reads) values. The RNA-Seq data were also deposited in the Gene Expression Omnibus (GEO accession No. GSE106370). The web-based tool DAVID (the Database for Annotation, Visualization, and Integrated Discovery) (Huang et al., 2009) was used to analyze the biological interpretation of DEGs, which were further classified according to Gene Ontology (GO) (Panther Ontology Database) as previously described (Sun et al., 2016).

Reverse transcription-associated quantitative PCR (RT-qPCR)

Total RNA was purified from the hypocotyls of the etiolated WT, mutant and transgenic seedlings using RNeasy Plant Mini Kit (Qiagen) as described previously (Yoon et al., 2016). Approximately 0.5 μg of purified RNA was used for cDNA synthesis using TOPscript™ RT DryMIX (dT18/dN6 plus) according to the manufacturer's instructions (Enzynomics, Korea), and then used as templates for RT-qPCR using Rb-Taq™ qPCR 2X PreMIX (Enzynomics) in the Mx3000P QPCR System (Agilent Technologies, USA) as previously described (Heo et al., 2011; Lee et al., 2016; Yoon et al., 2016). The *ACTIN2* (*ACT2*; AT3G18780) gene was used as an internal reference (Yoon et al., 2016). Each experiment was conducted independently at least three times for biological replicates. The error bars represent the SEM of biological triplicates. For dexamethasone (DEX) and cycloheximide (CHX) treatments, seedlings were grown on filter paper strips (~5 mm wide) in 0.5X MS agar plates for 6 days, transferred to new 0.5X MS agar plates supplemented with ethanol (control), 10 μM of DEX, or 10 μM of DEX with 10 μM of CHX, and then incubated for 3 h, 6 h, 12 h, or 24 h. The sequence information for RT-qPCR primers is listed in Supplementary Table S2.

Plasmid construction and plant transformation

To generate the transcriptional fusions of the three *XTH* genes (*ProXTH18::GUS*, *ProXTH22::GUS*, and *ProXTH24::GUS*), the putative promoter regions (the longest intergenic regions) of *XTH18* (~1.8-kb upstream region from the start codon), *XTH22* (~2.2-kb upstream region), and *XTH24* (~2.7-kb upstream region) were amplified from Columbia genomic DNA using Phusion high-fidelity DNA polymerase (Thermo Fisher Scientific, USA), and subcloned to pDONR221 according to the manufacturer's instructions (Thermo Fisher Scientific). Subsequently, the fragments were transferred to the Gateway compatible destination vector pMDC162 (Curtis and Grossniklaus, 2003) using the Gateway recombination cloning technology as previously described (Heo et al., 2011; Lee et al., 2016; Yoon et al., 2016). For overexpression of the *XTH* genes, the coding sequences of *XTH18* (849 bp), *XTH22* (855 bp), and *XTH24* (810 bp) were amplified from Columbia cDNA using Phusion high-fidelity DNA polymerase, and subcloned into pENTR/D-TOPO according to the manufacturer's instructions (Thermo Fisher Scientific). The error-free entry clones in the pENTR/D-TOPO vector were subsequently cloned into the pEarleyGate100 (Earley et al., 2006) as previously described (Heo et al., 2011; Lee et al., 2016; Yoon et al., 2016). To create the *ProSHR::SHR-nlsGFP* translational fusion, the MultiSite Gateway® cloning kit was used according to the manufacturer's instructions (Thermo Fisher Scientific). The promoter (~2.1-kb upstream region) and the coding region (1,596 bp) without stop codon were amplified using plasmids containing the *SHR* promoter (Yu et al., 2010) and its coding region, respectively. Subsequently, each fragment was subcloned into pDONR221 P1-P4 and pDONR221 P4r-P3r by BP recombination, respectively, according to the manufacturer's instructions (Thermo Fisher Scientific). The nuclear-localized version of GFP (*nlsGFP*) was amplified from the *ProWOL::SHRΔLNELDV-nlsGFP;shr-2* line (Carlsbecker et al., 2010), and subcloned into pDONR221 P3-P2 by BP recombination according to the manufacturer's instructions (Thermo Fisher Scientific). Finally, the *ProSHR::SHR-nlsGFP* fusion was transferred into pMDC123 (Curtis and Grossniklaus, 2003) by Gateway LR recombination as previously described (Heo et al., 2011; Lee et al., 2016; Yoon et al., 2016). For transient expression assays, the promoter regions of *XTH18* (835 bp upstream from the start codon), *XTH22* (460 bp upstream), and *XTH24* (1728 bp upstream) were inserted into the pBI221 reporter plasmid containing the firefly *LUC* gene as described previously (Lee et al., 2016; Yoon et al., 2016). The *35S* promoter was replaced by the promoter fragments of *XTH18*, *XTH22*, and *XTH24* in pBI221. To generate transgenic plants, Columbia plants were transformed using the floral dipping method (Clough and Bent, 1998). T_1 plants were selected by antibiotic- or herbicide-resistance, and subsequently T_2 homozygous plants were obtained through confirmation in the T_3 generation as described previously (Heo et al., 2011; Lee et al., 2016; Yoon et al., 2016). The sequence information of primers used for plasmid construction is listed in Supplementary Table S3.

GUS staining

Histochemical GUS staining of the hypocotyl was performed

using transgenic Arabidopsis plants carrying *ProXTH18::GUS*, *ProXTH22::GUS*, or *ProXTH24::GUS*. Seedlings were immersed in GUS staining solutions (0.4 mM X-Gluc, 2 mM $K_3Fe(CN)_6$, 2 mM $K_4Fe(CN)_6$, 0.1 M sodium phosphate, 10 mM EDTA, and 0.1% triton X-100) in the dark, and kept for 3 to 4 h at 37°C. The stained seedlings were cleared by dehydration through ethanol series (80%, 90%, and 100% EtOH) for 30 min each, and photographed using a digital camera (Olympus) as described previously (Yoon et al., 2016).

Transient expression assay

Transient expression assays were performed using WT or *shr-2 scr-5* protoplasts as previously described (Lee et al., 2016; Yoo et al., 2007; Yoon et al., 2016), with minor modifications. The protoplasts were prepared from 4-week-old rosette leaves using Cellulase R10 and Macerozyme R10 (Yakult Pharmaceuticals, Japan) as described previously (Lee et al., 2016; Yoon et al., 2016). The firefly luciferase (*LUC*) reporter and *Renilla LUC* reporter were employed as previously described (Lee et al., 2016; Yoon et al., 2016). Relative LUC activity was measured using the Dual-Luciferase Reporter Assay system (Promega, USA). The *GUS* gene driven by the *35S* promoter (*Pro35S::GUS*) in pBI221 was introduced as an internal control in each assay, and the background value obtained from the internal control was arbitrarily set to 1. Each experiment was independently repeated at least three times for biological replicates, and the data were analyzed using the Microsoft Excel program.

Chromatin immunoprecipitation-associated qPCR (ChIP-qPCR)

ChIP-qPCR experiments were performed as previously described (Cui et al., 2007; 2011; Yoon et al., 2016), with minor modifications. Approximately 1.5 g of the hypocotyls of 6-day-old etiolated *shr-2* and *shr-2 scr-5* seedlings harboring the *ProSHR::SHR-GFP* translational fusion were cross-linked in 1% formaldehyde solution (1% formaldehyde and 5 mM EDTA in 1X phosphate-buffered saline [PBS]) for 20 min under vacuum. To stop cross-linking, 100 mM glycine was added to the samples and incubated for 5 min. The samples were thoroughly washed in pre-chilled 1X PBS buffer with 5 mM EDTA. The cross-linked samples were pulverized in liquid nitrogen, and dissolved in extraction buffer (50 mM Tris pH 7.5, 150 mM NaCl, 1% Triton X-100, 0.1% sodium deoxychlorate, 2.5 mM EDTA, 10% glycerol, 1X protease inhibitor cocktail, and 1 mM PMSF). The nuclei preparation was sonicated using an EpiShear Probe Sonicator (Active Motif, USA) to break the chromatin threads into 0.5 to 1-kb fragments. An aliquot was obtained from each sample for the exclusive use of input. The anti-GFP antibody (cat. No. ab290; Abcam, USA) and protein A agarose beads (Millipore, USA) were used for immunoprecipitation of the sheared chromatin. The beads were successively washed away sequentially with low salt buffer (150 mM NaCl, 0.2% SDS, 0.5% Triton X-100, 2 mM EDTA, and 20 mM Tris-HCl [pH 8.0]), high salt buffer (500 mM NaCl, 0.2% SDS, 0.5% Triton X-100, 2 mM EDTA, and 20 mM Tris-HCl [pH 8.0]), LiCl washing buffer (0.25 M LiCl, 0.5% NP-40, 0.5% sodium deoxycholate, 1 mM EDTA, and 10 mM Tris-HCl [pH 8.0]), and TE buffer (10 mM Tris-HCl [pH 8.0] and 1 mM EDTA). The chromatin fragments were eluted in elution buffer (25 mM Tris [pH 8.0], 5 mM EDTA, and 0.5% SDS), were incubated overnight at 65°C, and subsequently treated with DNase-free RNase A (Sigma-Aldrich, USA) and proteinase K (Thermo Fisher Scientific). The DNA fragments were further purified using spin columns (Qiagen), eluted in 50 μl TE buffer, and used for qPCR. Both immunoprecipitated and input DNA samples were used for qPCR with an Mx3000P QPCR machine (Agilent Technologies) as described previously (Yoon et al., 2016). The known SHR-binding region of the *SCR* promoter was used as a positive control. Each experiment was performed at least three times for biological replicates. The sequence information for ChIP-qPCR primers is listed in Supplementary Table S4.

Hypocotyl graft experiment

Graft experiments were performed by using the roots and hypocotyls of 4-day-old etiolated WT and *shr-2* seedlings as previously described (Marsch-Martínez et al., 2013), with minor modifications. Initially, seedlings were grown on 0.5X MS agar plates supplemented with 0.5% sucrose for 4 days in the dark. To graft the WT hypocotyls onto the *shr-2* rootstocks or vice versa, seedlings were cut above 2 mm of the root-hypocotyl junction with a medical scalpel blade and the hypocotyls of WT and *shr-2* were swapped onto the rootstocks, respectively. As control experiments, the hypocotyls of WT and *shr-2* were grafted onto their own rootstocks (WT hypocotyls onto WT rootstocks or *shr-2* hypocotyls onto *shr-2* rootstocks). Subsequently, the grafted seedlings were kept in the dark for another 3 days and photographed with a digital camera (Olympus). The hypocotyl length of the survivors ($n > 30$) from the grafted seedlings was measured by using NIH Image J software, and the data were analyzed using the Microsoft Excel program. The graft experiments were performed in sterile conditions within a tissue culture hood.

Confocal microscopy

For confocal laser scanning microscopy, the roots of the light-grown seedlings were stained in 1 μM of propidium iodide (Sigma-Aldrich) for 2 min, and mounted in distilled water as described previously (Heo et al., 2011; Lee et al., 2016; Yoon et al., 2016). For the hypocotyls of the etiolated seedlings, the samples were stained in 1 μM of propidium iodide (Sigma-Aldrich) for 30 min. The images were obtained using a Zeiss LSM 800 microscope (Zeiss) as described previously (Heo et al., 2011; Lee et al., 2016; Yoon et al., 2016).

Hypocotyl gravity response assay

Gravitropic responses and amyloplast staining assays of the etiolated hypocotyls were performed as described previously (Fukaki et al., 1998; Yoon et al., 2016). For gravitropic response, seedlings were vertically grown on 0.5X MS agar plates without sucrose in the dark for 3 days, rotated to the clockwise direction by an angle of 90°, and incubated for 2 days as described previously (Yoon et al., 2016). The etiolated seedlings were collected and fixed overnight in FAA solution (10% formaldehyde, 5% acetic acid, and 50% ethanol). To visualize amyloplast sedimentation, the etiolated seedlings were washed in 50% (v/v) ethanol, stained in Lugol's

solution, and observed with DIC (differential interference contrast) optics using an Axio Imager.A1 microscope as described previously (Yoon et al., 2016).

Accession numbers

All the raw data generated in this work are deposited in the NCBI GEO database (http://www.ncbi.nlm.nih.gov/geo/) with the accession number: GSE97670 (ATH1 GeneChip microarrays) and GSE106370 (RNA-Seq). Sequence data from this paper can be found in the Arabidopsis Genome Initiative under the following accession numbers: *ACT2* (AT3G18780), *SHR* (AT4G37650), *SCR* (AT3G54220), *XTH1* (AT4G13080), *XTH2* (AT4G13090), *XTH3* (AT3G25050), *XTH4* (AT2G06850), *XTH5* (AT5G13870), *XTH6* (AT5G65730), *XTH7* (AT4G37800), *XTH8* (AT1G11545), *XTH9* (AT4G03210), *XTH10* (AT2G14620), *XTH11* (AT3G48580), *XTH12* (AT5G57530), *XTH13* (AT5G57540), *XTH14* (AT4G25820), *XTH15* (AT4G14130), *XTH16* (AT3G23730), *XTH17* (AT1G65310), *XTH18* (AT4G30280), *XTH19* (AT4G30290), *XTH20* (AT5G48070), *XTH21* (AT2G18800), *XTH22* (AT5G57560), *XTH23* (AT4G25810), *XTH24* (AT4G30270), *XTH25* (AT5G57550), *XTH26* (AT4G28850), *XTH27* (AT2G01850), *XTH28* (AT1G14720), *XTH29* (AT4G18990), *XTH30* (AT1G32170), *XTH31* (AT3G44990), *XTH32* (AT2G36870), and *XTH33* (AT1G10550).

RESULTS

SHR is required for hypocotyl cell elongation in the etiolated seedling

Our previous observation that the etiolated *shr* seedling exhibited a short-hypocotyl phenotype (Yoon et al., 2016) led us to hypothesize that SHR might play a role in the control of cell elongation. To test this, we performed a detailed phenotypic analysis on the etiolated hypocotyls of two null mutant seedlings, *shr-2* (Benfey et al., 1993; Helariutta et al., 2000) and *shr-6* (Yu et al., 2010). Under dark-grown conditions, the growth of *shr-2* and *shr-6* hypocotyls was retarded, as compared with that of the Columbia wild type (hereafter referred to as WT) (Figs. 1A-1C). It is well known that plant growth is driven by cell division and/or cell elongation (Beemster and Baskin, 1998; Sablowski, 2016; Sablowski and Gutierrez, 2021). We therefore measured the numbers and lengths of individual cells in the hypocotyls of 6-day-old etiolated WT and *shr* seedlings (see Materials and Methods section). To compare those parameters between WT and *shr*, we focused on the inner cortex cells along the longitudinal axis of the hypocotyl because the *shr* seedlings had no endodermis (Fukaki et al., 1998; Yoon et al., 2016) and the cortex cells were easier to measure than the stele cells. In both *shr-2* and *shr-6* etiolated seedlings, the cell numbers from the root-hypocotyl

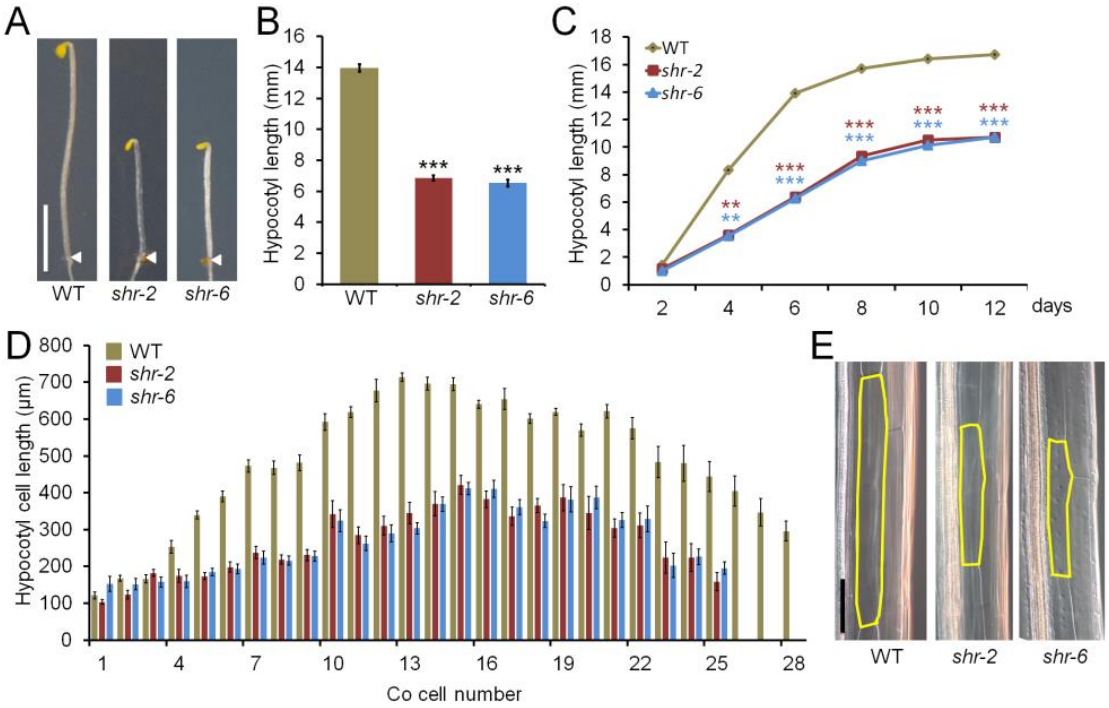

Fig. 1. Hypocotyl growth analysis of etiolated WT and *shr* seedlings. (A) Hypocotyls of 6-day-old etiolated WT, *shr-2*, and *shr-6* seedlings. The white arrowheads indicate the hypocotyl-root junction of the seedlings. Scale bar = 5 mm. (B) Hypocotyl lengths of the etiolated WT, *shr-2*, and *shr-6* seedlings. The data are shown as mean ± SEM (n > 30). (C) Hypocotyl growth of the etiolated WT, *shr-2*, and *shr-6* seedlings at different time points. The data are shown as mean ± SEM (n > 30). (D) Cortex (Co) cell numbers (x-axis) and cell lengths (y-axis) of the hypocotyls of 6-day-old etiolated WT, *shr-2*, and *shr-6* seedlings. We measured the numbers and lengths of the inner cortex cells in the hypocotyl ground tissue because both *shr-2* and *shr-6* had no endodermis. (E) The inner cortex cells of the hypocotyls of the etiolated WT, *shr-2*, and *shr-6* seedlings. The yellow borders outline the inner cortex cells. Scale bar = 100 μm. Statistical significance was determined by Student's *t*-test compared with the WT. $^{**}P < 0.01$; $^{***}P < 0.001$.

junction to the point just below the apical hook were not significantly different from those in the WT (~25 ± 3 cells vs ~28 ± 4 cells) (Fig. 1D). In contrast, the lengths of individual cells in *shr-2* and *shr-6* hypocotyls were discernibly reduced, in comparison with those in the WT (Figs. 1D and 1E). Because 13th to 15th cells from the root-hypocotyl junction were found to be most highly elongated (Fig. 1D), we assessed the lengths of 13th to 15th inner cortex cells in the hypocotyl for cell elongation hereafter. Under light-grown conditions, the hypocotyl lengths of *shr* seedlings were also shorter than those of the WT (Supplementary Fig. S1), suggesting that SHR plays a role in hypocotyl cell elongation in both light- and dark-grown seedlings. Further investigation on SHR in the light-grown seedling hypocotyl is the subject of another study and is not discussed further here.

Taken together, our results strongly support the idea that the short-hypocotyl phenotype of the etiolated *shr* seedlings is primarily due to a reduction in cell elongation, rather than in cell division.

SHR regulates expression of *XTH* genes in the etiolated hypocotyl

To understand the molecular events underlying the SHR-mediated control of cell elongation, we analyzed the expression profiles of 6-day-old etiolated WT and *shr-2* hypocotyls using ATH1 GeneChip microarrays and Next Generation Sequencing of RNA (RNA-Seq) (cutoff: > 1.5-fold and $P < 0.05$) (Supplementary Datasets S1 and S2). The DEGs were analyzed by the GO terms using DAVID resources (Huang et al., 2009; Supplementary Fig. S2A). Considering that cell wall modifications play vital roles in cell elongation (Chebli and Geitmann, 2017; Cosgrove, 2005; 2016a; 2016b), we were particularly interested in the DEGs belonging to the cell wall category in the "Cellular Component" GO domain (Supplementary Fig. S2A). Subsequently, we analyzed the DEGs in the cell wall category using the "Molecular Function" and "Biological Process" GO terms. Of the candidate genes, we found that the *XTH* genes, which encode cell wall remodeling enzymes, had high enrichment scores from our GO analysis (Supplementary Figs. S2B and S2C).

In the Arabidopsis genome (TAIR v10), 33 *XTH* genes have been identified, ranging from group I to III (Eklöf and Brumer, 2010; Lee et al., 2005; Rose et al., 2002; Yokoyama and Nishitani, 2001). We found that 23 of these genes were differentially regulated between WT and *shr-2* hypocotyls (Supplementary Fig. S3A, Supplementary Dataset S3). Next, we conducted RT-qPCR experiments to verify the results from our transcriptomic analysis. Regarding group I, the transcript levels of five *XTH* genes were significantly changed in *shr-2* (*XTH4* and *XTH7* were down-regulated, whereas *XTH5*, *XTH9* and *XTH10* were up-regulated; Supplementary Fig. S3B). In group II, the levels of *XTH17*, *XTH18*, *XTH19*, *XTH23*, and *XTH24* expression were evidently reduced, whereas those of *XTH12*, *XTH14*, *XTH15*, *XTH16* and *XTH20* were elevated in *shr-2* hypocotyls (Supplementary Fig. S3C). Among group III, the mRNA levels of four *XTH* genes were discernibly modulated in *shr-2* (*XTH30* and *XTH31* were down-regulated, while *XTH32* and *XTH33* were up-regulated; Supplementary Fig. S3D). Considering the differences between the two expression analysis platforms (ATH1 microarrays vs RNA-Seq), we extended our RT-qPCR analysis to the remaining *XTH* genes. Of the remaining *XTH* genes in group I, expression of three *XTH* genes was significantly changed (transcription of *XTH6* was attenuated, whereas that of *XTH8* and *XTH11* was promoted; Supplementary Fig. S4A). In group II, the *XTH22* expression level was reduced, while both *XTH21* and *XTH25* levels were elevated in *shr-2* (Supplementary Fig. S4B). We found no obvious change in the *XTH29* transcript level, which was the only remaining *XTH* gene in group III (Supplementary Fig. S4C). Overall, in combination of transcriptomic and RT-qPCR analyses, a total of 11 *XTH* genes (*XTH4*, *XTH6*, *XTH7*, *XTH17*, *XTH18*, *XTH19*, *XTH22*, *XTH23*, *XTH24*, *XTH30*, and *XTH31*) were down-regulated in the etiolated *shr-2* hypocotyl.

Given the short-hypocotyl phenotype of the etiolated *shr* seedling, we assumed that the loss of SHR function caused the observed reduction in the *XTH* gene expression levels in the etiolated *shr-2* hypocotyl. To investigate this hypothesis, we used Arabidopsis transgenic plants carrying an inducible version of SHR in the *shr-2* background (*ProSHR::SHR-GR;shr-2*). In the hypocotyl, the expression of *XTH17*, *XTH18*, *XTH22*, and *XTH24* was promoted when SHR was induced by dexamethasone treatment (+DEX) at 3, 6, 12, and 24 h (Supplementary Fig. S5). We further found that the levels of *XTH18*, *XTH22*, and *XTH24* transcripts were elevated in the hypocotyl upon dexamethasone- and cycloheximide- (DEX + CHX) induced SHR at 6 h (Supplementary Fig. S6). Thus, these results indicate that SHR activates transcription of *XTH18*, *XTH22*, and *XTH24* in the etiolated hypocotyl.

To further verify SHR-mediated activation of these three *XTH* genes in the hypocotyl, we monitored the *in planta* expression patterns using transcriptional GUS fusions (*ProXTH18::GUS*, *ProXTH22::GUS*, and *ProXTH24::GUS*). Similar to the *ProSHR::GUS* fusion, the expression of the three GUS fusions was detected in the hypocotyl stele (Supplementary Fig. S7). Next, we examined their expression patterns in etiolated WT and *shr-6* hypocotyls. Compared with those in the WT, the three *XTH* fusions were down-regulated in *shr-6* (Figs. 2A-2C). In addition, we performed transient expression assays using Arabidopsis protoplasts, and found that the *LUC* expression, driven by the promoters of the three *XTH* genes (*ProXTH18::LUC*, *ProXTH22::LUC*, and *ProXTH24::LUC*), was elevated upon SHR introduction as an effector (Figs. 2D and 2E). Next, to determine whether SHR directly activates transcription of these *XTH* genes, we employed ChIP-qPCR using the etiolated hypocotyls of *shr-2* seedlings with the mobile version of SHR driven by the native SHR promoter (*ProSHR::SHR-GFP;shr-2*), which was shown to rescue the *shr* phenotypes in roots and shoots (Carlsbecker et al., 2010; Gallagher and Benfey, 2009; Gallagher et al., 2004; Nakajima et al., 2001; Yoon et al., 2016). Indeed, SHR binding to the *XTH* promoter regions was enriched (Figs. 2F-2H). Taken together, our findings indicate that SHR, being associated with the promoters, activates the transcription of the three *XTH* genes in the etiolated Arabidopsis hypocotyl.

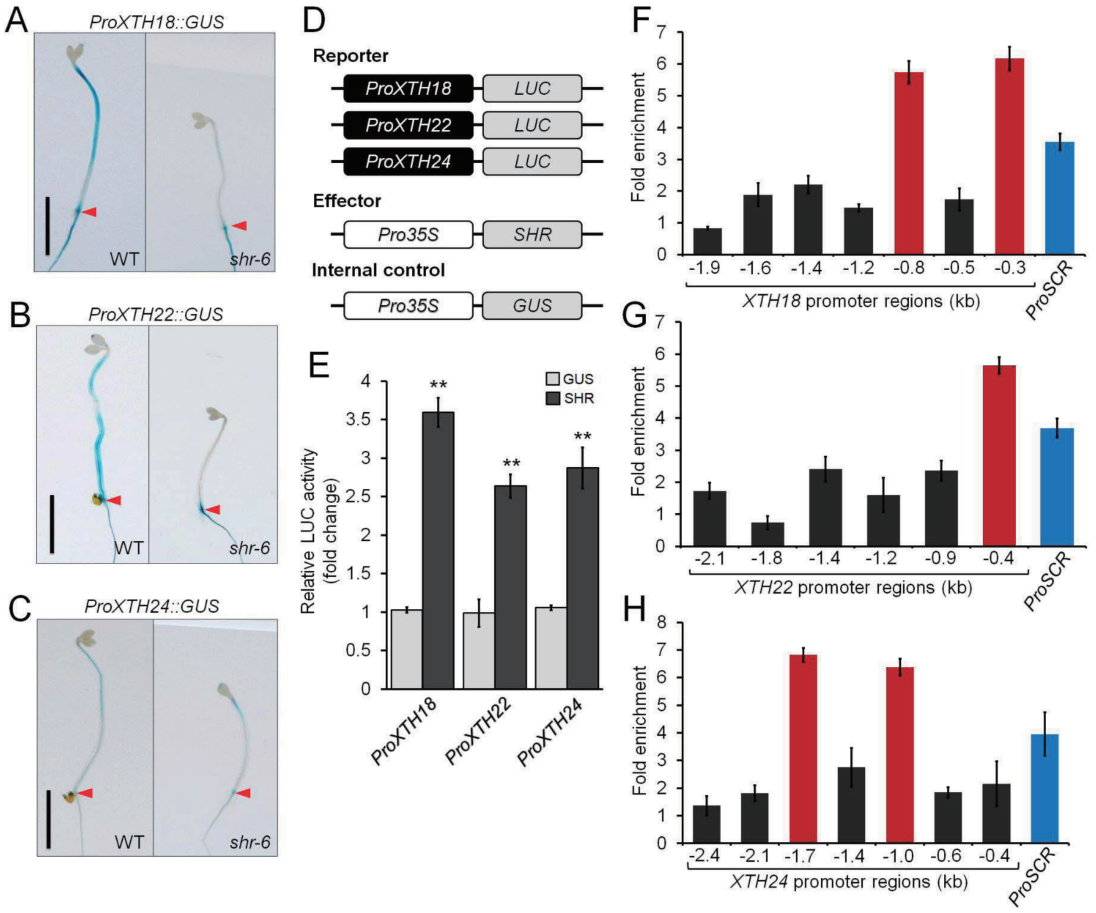

Fig. 2. Transcriptional regulation of *XTH18*, *XTH22*, and *XTH24* by SHR in the etiolated hypocotyl. (A-C) The *in planta* expression patterns of *ProXTH18::GUS* (A), *ProXTH22::GUS* (B), and *ProXTH24::GUS* (C) in the hypocotyls of 6-day-old etiolated WT and *shr-6* seedlings. The red arrowheads indicate the hypocotyl-root junction of the seedlings. Scale bars = 5 mm. (D) Schematic illustration for the reporter and effector plasmids used for the transient expression assays using Arabidopsis WT protoplasts. The reporter plasmids consist of the *XTH18*, *XTH22*, and *XTH24* promoter regions, which drive the transcription of the firefly luciferase (*LUC*) gene. The effector plasmid carries the *SHR* coding sequence with the 35S promoter (*Pro35S::SHR*). The *Pro35S::GUS* plasmid was used as an internal control. (E) The relative LUC activity driven by the three *XTH* promoters was measured when SHR was introduced. The value of *ProXTH18::LUC*, *ProXTH22::LUC*, and *ProXTH24::LUC* in the presence of the *Pro35S::GUS* internal control was set to 1. Error bars indicate mean ± SEM of three biological replicates. Statistical significance was determined by Student's *t*-test compared with the internal control. $**P < 0.01$. (F-H) ChIP-qPCR assays using 6-day-old etiolated *shr-2* seedlings with the *ProSHR::SHR-GFP* translational fusion (*ProSHR::SHR-GFP;shr-2*). Error bars indicate mean ± SEM of three biological replicates. The prominent SHR-binding regions were highlighted red when the enrichment values of SHR binding to the promoter regions of *XTH18* (F), *XTH22* (G), and *XTH24* (H) were higher than those of the known SHR-binding region in the *SCR* promoter (*ProSCR* as a positive control; shown as blue).

Overexpression of *XTH18*, *XTH22*, and *XTH24* can promote cell elongation in the etiolated hypocotyl

To understand the SHR-mediated regulation of the *XTH* genes in hypocotyl growth, we first isolated T-DNA insertion mutants for *XTH18*, *XTH22*, and *XTH24* (http://signal.salk.edu; Supplementary Figs. S8A and S8B). Unfortunately, the loss-of-function mutants of these *XTH* genes displayed no visible phenotype in hypocotyl growth (Supplementary Figs. S8C and S8D). Furthermore, we found that the hypocotyl length of the triple mutant (*xth18-1 xth22-2 xth24-1*) was indistinguishable from that of the WT (Supplementary Figs. S8E and S8F), suggesting that these genes are highly redundant in function.

Alternatively, we generated Arabidopsis transgenic plants, which overexpressed these *XTH* genes (*XTH-OXs*), under the *35S* cauliflower mosaic virus (*35S* CaMV) promoter (Supplementary Fig. S9A). In agreement with previous work (Miedes et al., 2013), the hypocotyls of *XTH18* overexpression lines (*XTH18-OX* #7 and #10) were longer than those of WT under dark-grown conditions (Supplementary Figs. S9B and S9C). We also found that overexpression of *XTH22* (*XTH22-OX* #6 and #14) and *XTH24* (*XTH24-OX* #8 and #9) resulted in longer hypocotyls (Supplementary Figs. S9B and S9C). Further microscopic analyses revealed that individual cells in the etiolated hypocotyls of the overexpression lines were more elongated than those in the WT (Supplementary Figs. S9D

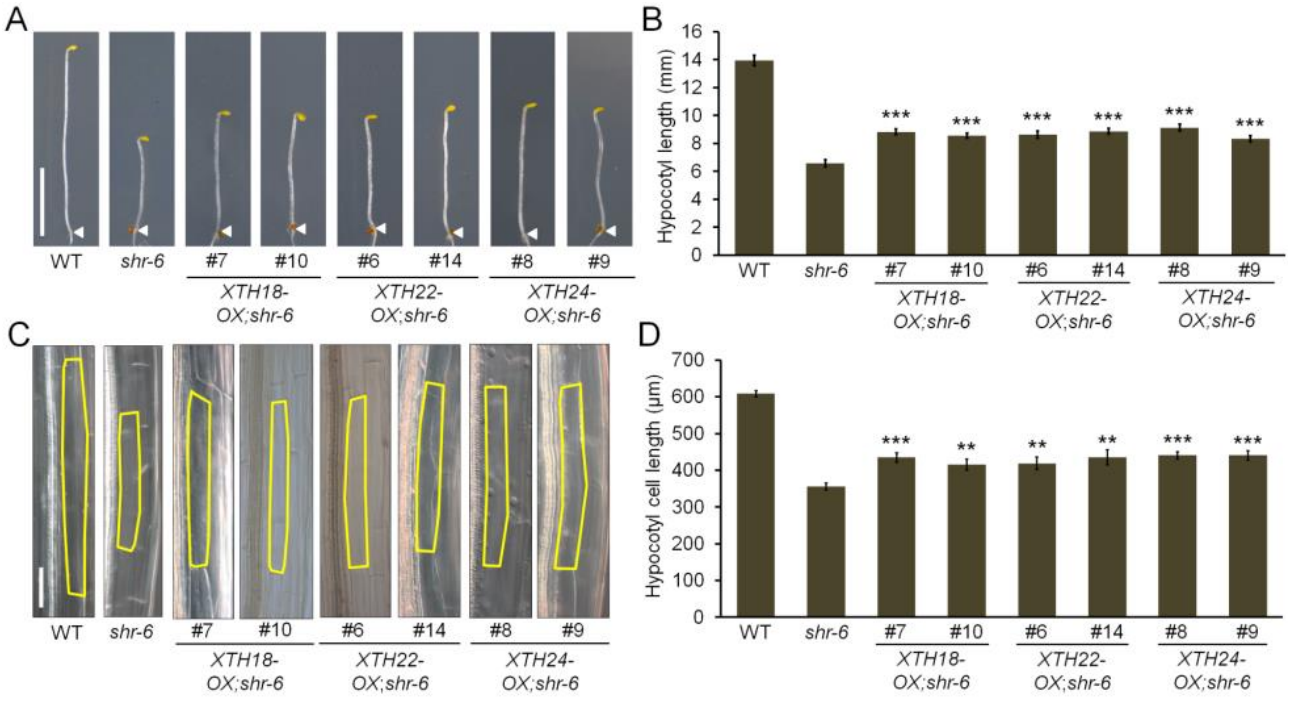

Fig. 3. Overexpression of *XTH18*, *XTH22*, and *XTH24* in *shr* hypocotyls. (A and B) Hypocotyl growth of 6-day-old etiolated WT, *shr-6*, and *shr-6* carrying *XTH18-OX* (*XTH18-OX;shr-6* #7 and #10), *XTH22-OX* (*XTH22-OX;shr-6* #6 and #14), or *XTH24-OX* (*XTH24-OX;shr-6* #8 and #9) seedlings. The white arrowheads indicate the hypocotyl-root junction of the etiolated seedlings. Scale bar = 5 mm. (C and D) Hypocotyl cell elongation of 6-day-old etiolated WT, *shr-6*, *XTH18-OX;shr-6* (#7 and #10), *XTH22-OX;shr-6* (#6 and #14), and *XTH24-OX;shr-6* (#8 and #9) seedlings. The yellow borders outline the inner cortex cells. Scale bar = 100 μm. For bar graphs in (B and D), the data are shown as mean ± SEM (n > 30). Statistical significance was determined by Student's *t*-test compared with *shr-6*. $^{**}P < 0.01$; $^{***}P < 0.001$.

and S9E). Subsequently, to investigate whether *XTH* overexpression could rescue the short-hypocotyl phenotype caused by the loss of SHR function, we introduced the *XTH18-OX*, *XTH22-OX* and *XTH24-OX* transgenes, respectively, into the *shr-6* background. Compared with the *shr-6* single mutant, the etiolated *shr-6* seedlings carrying *XTH18-OX* (*XTH18-OX;shr-6*), *XTH22-OX* (*XTH22-OX;shr-6*), or *XTH24-OX* (*XTH24-OX;shr-6*) exhibited visibly slight but statistically significant hypocotyl cell elongation (Figs. 3A and 3B). In microscopic analyses, we also observed that the overexpression lines had more elongated cells than those in the *shr-6* hypocotyls (Figs. 3C and 3D).

Taken together, our finding indicates that overexpression of each *XTH* gene in the *shr-6* background was capable of promoting cell elongation, but failed to completely restore the short-hypocotyl phenotype to the WT level. Thus, it is likely that the SHR-mediated regulation of cell elongation in the etiolated hypocotyl is far more complex than it looks.

SHR activates the expression of *XTH18*, *XTH22*, and *XTH24* in a SCR-independent manner

In most developmental processes, SHR is known to act together with SCR to activate the expression of the target genes (Carlsbecker et al., 2010; Cruz-Ramírez et al., 2012; Cui et al., 2007; Dhondt et al., 2010; Helariutta et al., 2000; Hirano et al., 2017; Koizumi et al., 2012a; 2012b; Levesque et al., 2006; Sozzani et al., 2010; Yoon et al., 2016). Thus, to determine whether SCR is also involved in the SHR-mediated hypocotyl growth, we first examined the etiolated *scr-5* hypocotyl. Under dark-grown conditions, the etiolated *scr-5* seedling also showed a short-hypocotyl phenotype (~11.2 ± 0.23 mm) compared with the WT (~14.6 ± 0.22 mm); however, its hypocotyl length was longer than that of *shr-2* (~7.1 ± 0.28 mm) (Supplementary Fig. S10A). We further found that on average, the individual cell length in the *scr-5* hypocotyl (~474.5 ± 6.4 μm) was shorter than that of WT (~604.8 ± 13.8 μm), but longer than that of *shr-2* (~352.2 ± 8.7 μm) (Supplementary Fig. S10B). Next, we measured the hypocotyl length of the etiolated *shr-2 scr-5* double mutant seedling harboring the *ProSHR::SHR-GFP* fusion (*ProSHR::SHR-GFP;shr-2 scr-5*), and found that its hypocotyl length was nearly identical to that of the *scr-5* single mutant (Supplementary Fig. S10). In agreement with these phenotypic analyses, we observed that there was no significant difference in the mRNA levels of the three *XTH* genes between *scr-5* and *ProSHR::SHR-GFP;shr-2 scr-5* hypocotyls (Fig. 4A). We also performed transient expression assays using protoplasts from the *shr-2 scr-5* double mutant. Interestingly, SCR alone failed to promote the *LUC* expression driven by the *XTH* promoters in the *shr-2 scr-5* background (Figs. 4B and 4C). In contrast, the *LUC* expression was highly induced when only SHR was used as an effector (Fig. 4C). Moreover, when both SHR and

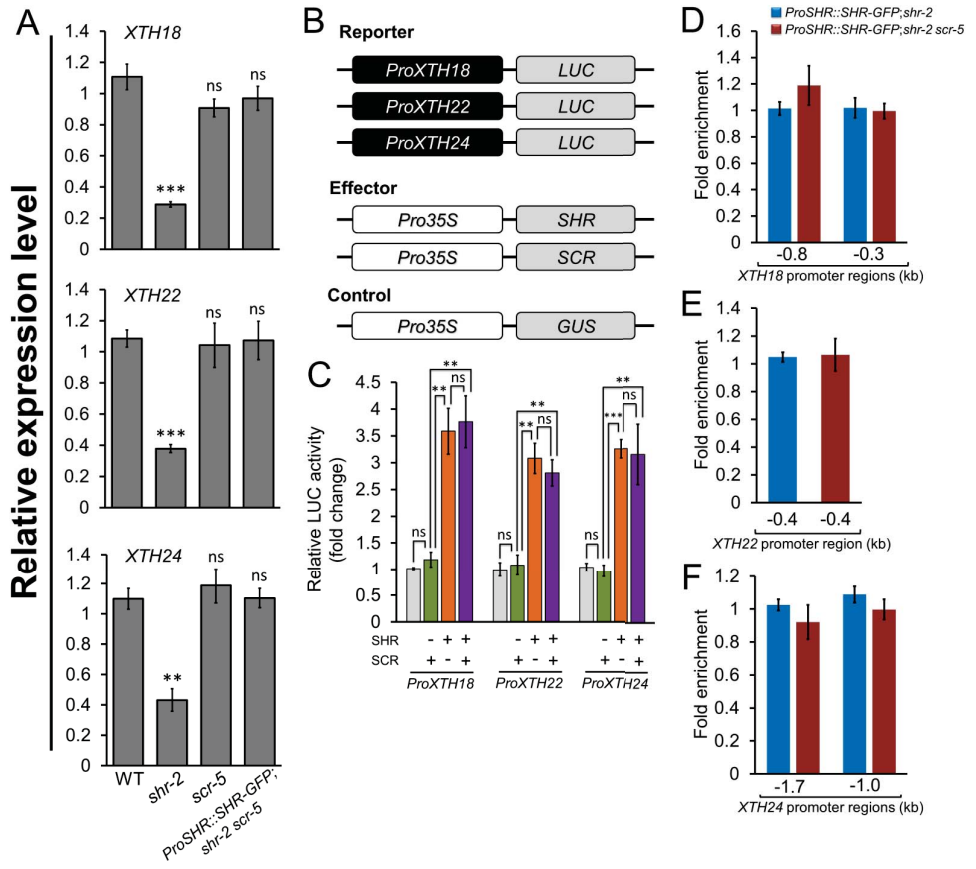

Fig. 4. Transcriptional regulation of *XTH18*, *XTH22*, and *XTH24* by SHR in a SCR-independent manner. (A) Transcript levels of the three *XTH* genes in the hypocotyls of 6-day-old etiolated WT, *shr-2*, *scr-5*, and *ProSHR::SHR-GFP;shr-2 scr-5* seedlings. The value for the WT was set to 1 and the relative values to the WT were shown. Error bars indicate mean ± SEM of three biological replicates. Statistical significance was determined by Student's *t*-test compared with the WT. $**P < 0.01$; $***P < 0.001$; ns, statistically not significant. (B) Schematic illustration of the effector and reporter constructs used for the transient expression assays using Arabidopsis protoplasts from the *shr-2 scr-5* double mutant. The promoter regions of the three *XTH* genes were fused to the firefly *LUC* gene (*ProXTH18::LUC*, *ProXTH22::LUC*, or *ProXTH24::LUC*). The effector plasmids consist of the coding regions of either *SHR* or *SCR* under the control of the *35S* promoter (*Pro35S::SHR* or *Pro35S::SCR*). The *Pro35S::GUS* construct was used as an internal control. (C) The relative LUC activity was measured in the presence of SCR alone (green), SHR alone (orange), or both SCR and SHR (purple). The value of *ProXTH18::LUC*, *ProXTH22::LUC*, and *ProXTH24::LUC* in the presence of the *Pro35S::GUS* internal control was set to 1 (light gray), respectively. Error bars indicate mean ± SEM of three biological replicates. Statistical significance was determined by Student's *t*-test. $**P < 0.01$; $***P < 0.001$; ns, statistically not significant. (D-F) ChIP-qPCR assays for SHR binding to the promoter regions of *XTH18* (D), *XTH22* (E), and *XTH24* (F) using the hypocotyls of etiolated *ProSHR::SHR-GFP;shr-2* (blue) and *ProSHR::SHR-GFP;shr-2 scr-5* (red) seedlings. Error bars indicate mean ± SEM of three biological replicates. The SHR-enriched fragments of the *ProSHR::SHR-GFP;shr-2 scr-5* line were nearly indistinguishable from those of the *ProSHR::SHR-GFP;shr-2* control line.

SCR were introduced into *shr-2 scr-5* protoplasts, LUC activity was indistinguishable from that in the SHR-only case (Fig. 4C). To further investigate whether SHR without its partner SCR directly activates the expression of the *XTH* genes, we performed ChIP-qPCR using *ProSHR::SHR-GFP;shr-2 scr-5* seedlings, along with the *ProSHR::SHR-GFP;shr-2* line as a control. As seen in the *ProSHR::SHR-GFP;shr-2 scr-5* hypocotyl, enrichment of SHR binding to the *XTH* promoter fragments was similar to that of the *ProSHR::SHR-GFP;shr-2* control line (Figs. 4D-4F). Therefore, our results indicate that unlike the canonical SHR-mediated transcriptional regulation (Cui et al., 2007; Cruz-Ramírez et al., 2012; Hirano et al., 2017; Koizumi et al., 2012a; 2012b; Yoon et al., 2016), SHR does not require its partner SCR to activate the transcription of the three *XTH* genes in the etiolated hypocotyl.

Restriction of SHR movement reveals that hypocotyl growth can be uncoupled from radial patterning

The *shr* mutant showed defective patterning and determinate growth in the root (Benfey et al., 1993; Helariutta et al., 2000; Sozzani et al., 2010). Thus, it is considered that both SHR-mediated patterning and growth may be tightly linked in the Arabidopsis root. To date, the non-cell-autonomous function of SHR has been extensively studied (Carlsbecker et

al., 2010; Clark et al., 2016; Cui et al., 2007; Gallagher and Benfey, 2009; Gallagher et al., 2004; Koizumi et al., 2012a; 2012b; Nakajima et al., 2001). Nevertheless, the cell-autonomous SHR pathway, which likely exists and operates in the stele, is poorly understood.

Before investigating the role of SHR in the hypocotyl stele, we first evaluated whether the short-hypocotyl phenotype of the etiolated *shr* seedling was due to defective root growth and development. We thus conducted grafting experiments by reciprocally swapping WT hypocotyls and roots with those of *shr-2* mutants. When the *shr-2* hypocotyl was grafted onto the WT root stock, the short-hypocotyl phenotype was nearly indistinguishable from the control (*shr* hypocotyl grafted onto the *shr* root stock) (Supplementary Fig. S11). Likewise, we found no significant difference in hypocotyl elongation when the WT hypocotyl was grafted onto the *shr* root stock compared with the control (WT hypocotyl grafted onto the WT root stock) (Supplementary Fig. S11). These results suggest that reduced hypocotyl growth in the etiolated *shr* seedling is primarily attributable to hypocotyl defects, rather than to root defects.

Previously, we demonstrated that confinement of SHR protein in the hypocotyl stele was unable to restore the radial organization of the ground tissue, which resulted in a loss of the functional endodermis in the hypocotyl (Yoon et al., 2016). In addition, given that the etiolated *shr* seedling showed a reduction in hypocotyl growth (Fig. 1), we hypothesized that as seen in the root, SHR-mediated patterning and growth might also be coupled in the hypocotyl. To test this, we generated Arabidopsis transgenic plants with a non-mobile version of SHR by adding a nuclear-localization signal to GFP under the control of the SHR promoter (*Pro-*

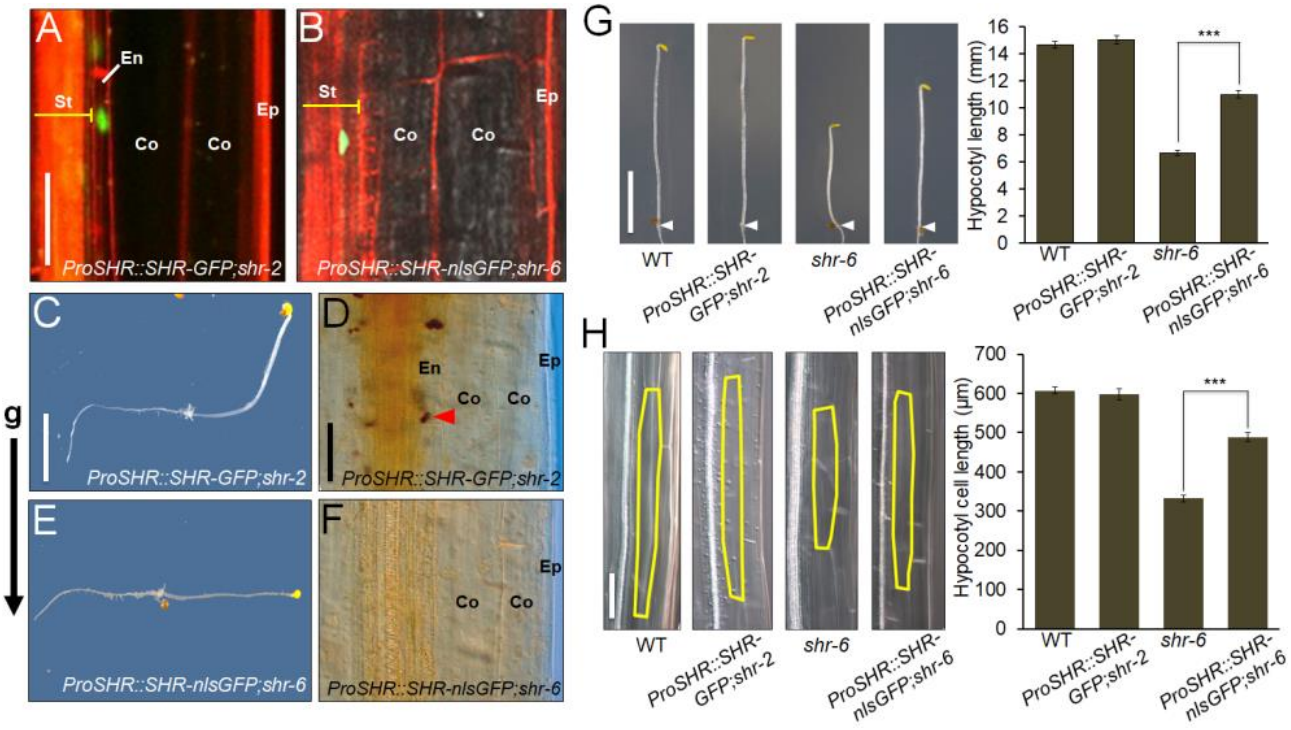

Fig. 5. Confinement of SHR in the stele is capable of promoting hypocotyl growth. (A and B) Confocal images of the etiolated *ProSHR::SHR-GFP* (A) and *ProSHR::SHR-nlsGFP* (B) hypocotyls. While the mobile SHR-GFP recombinant proteins were found in both hypocotyl stele and endodermis (A), the non-mobile SHR-nlsGFP proteins were localized only in the stele (B). The epidermis (Ep), cortex (Co), endodermis (En), and stele (St) are indicated. Scale bar = 70 μm. (C-F) Gravitropic responses and amyloplast staining of the etiolated *ProSHR::SHR-GFP* (C and D) and *ProSHR::SHR-nlsGFP* (E and F) hypocotyls. Three-day-old etiolated seedlings were rotated by an angle of 90° and incubated for 2 days. The arrow indicates the direction of gravity (g). While the *ProSHR::SHR-GFP* hypocotyl exhibited a normal gravitropic response (C), the *ProSHR::SHR-nlsGFP* hypocotyl was agravitropic (E). Amyloplasts were found to be precipitated at the bottom of the endodermis cells of the *ProSHR::SHR-GFP;shr-2* hypocotyl in response to the change of gravity vector (D). In contrast, no amyloplast sedimentation was observed in the *ProSHR::SHR-nlsGFP;shr-6* hypocotyl because there was no functional endodermis in the *ProSHR::SHR-nlsGFP;shr-6* hypocotyl (F). The red arrowhead indicates amyloplast sedimentation in the endodermis. Scale bars = 5 mm (C) and 70 μm (D). (G) Hypocotyl growth of 6-day-old etiolated WT, *ProSHR::SHR-GFP;shr-2*, *shr-6*, and *ProSHR::SHR-nlsGFP;shr-6* seedlings. The non-mobile SHR in the stele (*ProSHR::SHR-nlsGFP*) was able to restore the hypocotyl length of *shr-6* to ~80% of the WT and *ProSHR::SHR-GFP;shr-2* hypocotyl lengths. The white arrowheads indicate the hypocotyl-root junction of the seedlings. Scale bar = 5 mm. (H) Hypocotyl cell elongation of 6-day-old etiolated WT, *ProSHR::SHR-GFP;shr-2*, *shr-6*, and *ProSHR::SHR-nlsGFP;shr-6* seedlings. The yellow borders outline the inner cortex cells. Scale bar = 100 μm. For bar graphs in (G and H), the data are shown as mean ± SEM (n > 30). Statistical significance was determined by Student's *t*-test compared with *shr-6*. ***$P < 0.001$.

SHR::SHR-nlsGFP), which was shown to sufficiently restrict SHR movement from the stele (Gallagher et al., 2004; Gallagher and Benfey, 2009). We introduced this transgene into the *shr-6* background (*ProSHR::SHR-nlsGFP;shr-6*) by genetic crosses. Unlike the *ProSHR::SHR-GFP;shr-2* control line, the *ProSHR::SHR-nlsGFP;shr-6* root showed defective patterning and determinate growth (Supplementary Fig. S12). In agreement with previous work (Gallagher and Benfey, 2009; Gallagher et al., 2004; Yoon et al., 2016), restriction of SHR movement from the stele to the adjacent cells (e.g., endodermis, ground tissue stem cells, and quiescent center) failed to rescue the patterning and growth defects of the *shr* root.

Next, we extended our analysis to the etiolated hypocotyls of the *ProSHR::SHR-nlsGFP;shr-6* and *ProSHR::SHR-GFP;shr-2* seedlings. Unlike the *ProSHR::SHR-GFP;shr-2* line, the non-mobile SHR in *ProSHR::SHR-nlsGFP;shr-6* seedlings was unable to restore the radial patterning defects in *shr-6*, resulting in no response to a change in the gravity vector (Figs. 5A-5F). This finding is in agreement with previous report that the SHR-mediated patterning pathway is likely conserved in both root and hypocotyl (Kim et al., 2017; Yoon et al., 2016). Intriguingly, we found that the etiolated *ProSHR::SHR-nlsGFP;shr-6* hypocotyl was still elongated, which was comparable to ~80% of the WT and *ProSHR::SHR-GFP;shr-2* hypocotyl cell lengths (Figs. 5G and 5H). To determine whether the non-mobile SHR could induce hypocotyl growth via transcriptional activation of *XTH18*, *XTH22*, and *XTH24* in the stele, we analyzed the *XTH* transcript levels in the etiolated WT, *shr-6*, and *ProSHR::SHR-nlsGFP;shr-6* hypocotyls. Compared with that in *shr-6*, the expression of the three *XTH* genes in the *ProSHR::SHR-nlsGFP;shr-6* hypocotyl was induced to the WT levels (Supplementary Fig. S13).

Taken together, we demonstrated that the stele-localized non-mobile version of SHR was capable of promoting hypocotyl growth in the etiolated *ProSHR::SHR-nlsGFP;shr-6* seedling despite the patterning defects, potentially via transcriptional activation of the *XTH* genes in the stele. Therefore, it is tempting to speculate that the SHR-mediated growth pathway is uncoupled from the SHR-mediated patterning pathway in the etiolated hypocotyl.

DISCUSSION

To date, it is known that SHR, as a mobile transcription factor, plays a crucial role in controlling cell division for patterning and growth in Arabidopsis roots and shoots (Benfey et al., 1993; Carlsbecker et al., 2010; Cruz-Ramírez et al., 2012; Cui et al., 2007; Dhondt et al., 2010; Gallagher and Benfey, 2009; Gallagher et al., 2004; Gardiner et al., 2011; Helariutta et al., 2000; Koizumi et al., 2012a; 2012b; Levesque et al., 2006; Lucas et al., 2011; Nakajima et al., 2001; Sozzani et al., 2010; Yoon et al., 2016). For nearly two decades, researchers have further elucidated the molecular characteristics and regulatory roles of SHR in the root, which have thus become fundamental and prevalent research topics. However, our understanding of SHR function in the shoot remains superficial.

In this study, we reveal that in addition to its role in cell division, SHR is critically involved in controlling cell elongation of the etiolated Arabidopsis hypocotyl. To elucidate the molecular events underlying the SHR-mediated regulation of cell elongation, we employed genome-wide transcriptomic analyses using 6-day-old etiolated WT and *shr-2* hypocotyls, and identified a group of *XTH* genes which encode cell wall remodeling enzymes, as the candidate DEGs. Through extensive expression analyses, we found that SHR activated transcription of three group II *XTH* genes (*XTH18*, *XTH22*, and *XTH24*), as it was associated with their promoters, in the etiolated hypocotyl.

Unfortunately, likely due to their functional redundancy, even the triple mutant (*xth18-1 xth22-2 xth24-1*) did not show discernible phenotype in hypocotyl growth. Consistent with previous work (Miedes et al., 2013), overexpression of

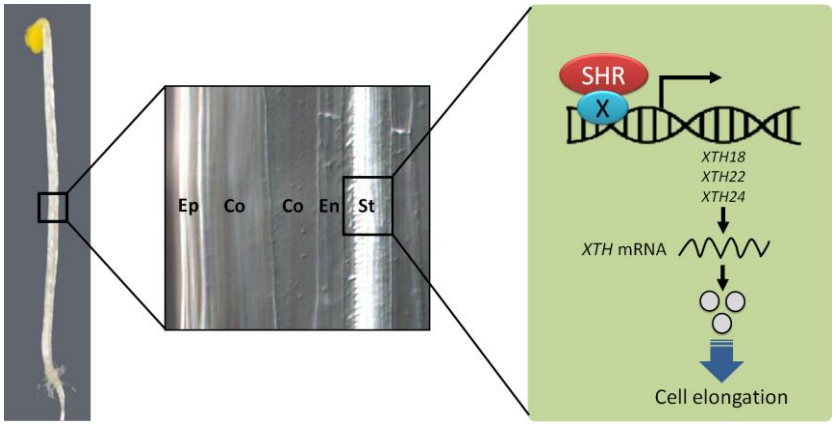

Fig. 6. A schematic model for the SHR-mediated regulation of hypocotyl cell elongation. SHR, being associated with the promoters of *XTH18*, *XTH22*, and *XTH24* genes, activates the transcription of the three *XTH* genes in the hypocotyl stele. SHR likely requires a partner (designated as protein X), which has DNA-binding activity, to promote the expression of the *XTH* genes because SHR has no canonical DNA binding motif. SCR, the interacting partner of SHR, is not involved in this process. Once *XTH18*, *XTH22*, and *XTH24* genes are expressed, these cell wall remodeling enzymes likely play roles in selective loosening and remodeling of cell walls for cell elongation in the etiolated Arabidopsis hypocotyl.

these *XTH* genes was able to promote cell elongation in both etiolated WT and *shr-6* hypocotyls. Nevertheless, overexpression of the *XTH* genes, respectively, in the *shr* background could not completely induce hypocotyl cell elongation to the WT level. This finding suggests that other factors-mediated regulatory networks play also crucial roles in hypocotyl growth (e.g., light conditions, plant hormones and/or expansins) (Bai et al., 2012; Cosgrove, 2005, 2016a, 2016b; De Lucas et al., 2008; Feng et al., 2008; Oh et al., 2014).

Interestingly, we found that the mode of the transcriptional regulation of the three *XTH* genes differed from the mode involved in root development. In the canonical mode of action, SHR forms protein complexes with its partner SCR transcription factor to modulate the expression of downstream target genes (Carlsbecker et al., 2010; Cruz-Ramírez et al., 2012; Cui et al., 2007; Gallagher and Benfey, 2009; Gallagher et al., 2004; Helariutta et al., 2000; Hirano et al., 2017; Kim et al., 2017; Koizumi et al., 2012a; 2012b; Levesque et al., 2006; Nakajima et al., 2001; Sozzani et al., 2010; Yoon et al., 2016). However, the levels of *XTH18*, *XTH22*, and *XTH24* transcripts and SHR binding to their promoters were not significantly changed in the *shr-2 scr-5* double mutant containing the *ProSHR::SHR-GFP* transgene (*ProSHR::SHR-GFP;shr-2 scr-5*). Our transient expression assays using *shr-2 scr-5* further corroborated that SHR alone was able to induce the expression of the *XTH* genes. Therefore, it is likely that SHR does not require SCR for transcriptional activation of these *XTH* genes. Considering that SHR itself contains no DNA binding motif (Di Laurenzio et al., 1996; Hirano et al., 2017; Pysh et al., 1999; Yoon et al., 2016), it is tempting to speculate that SHR interacts with other transcription factors (illustrated as protein X in Fig. 6) to promote the transcription of the three *XTH* genes for hypocotyl elongation (Fig. 6).

Previous studies demonstrated that intercellular movement of SHR is essential for the patterning of root development (Cui et al., 2007; Gallagher and Benfey, 2009; Gallagher et al., 2004; Helariutta et al., 2000; Kim et al., 2017; Koizumi et al., 2012a; 2012b; Nakajima et al., 2001; Yoon et al., 2016). In addition to patterning defects, the root growth of *shr* is markedly reduced (Benfey et al., 1993; Helariutta et al., 2000; Sozzani et al., 2010), implying that the SHR-mediated patterning and growth processes are tightly linked. To unravel the relationship between SHR-mediated patterning and growth in the etiolated hypocotyl, we generated *shr* plants harboring a non-mobile version of SHR in the nuclei of the stele cells (*ProSHR::SHR-nlsGFP;shr-6*). Consistent with previous studies (Carlsbecker et al., 2010; Gallagher et al., 2004), we found that restricting SHR movement into the adjacent cells did not rescue the patterning defects of both ground tissue and quiescent center in the root. Similarly, in the *ProSHR::SHR-nlsGFP;shr*-6 hypocotyl, we observed the aberrant radial organization with no endodermis, resulting in neither amyloplast sedimentation nor gravitropic response. Nonetheless, the stele-localized non-mobile version of SHR was still able to promote cell elongation in the *ProSHR::SHR-nlsGFP;shr*-6 hypocotyl, which was ~80% of the WT and *ProSHR::SHR-GFP;shr*-2 hypocotyl lengths. We also found that the non-mobile SHR could sufficiently induce the expression of *XTH18*, *XTH22*, and *XTH24* to the WT levels. These findings suggest that i) the autonomous SHR pathway exists and operates in the hypocotyl stele, and ii) SHR-mediated growth is uncoupled from SHR-mediated patterning. In addition, the result that the restoration of the stele-specific induction of the *XTH* genes in the *ProSHR::SHR-nlsGFP;shr*-6 hypocotyl failed to complement hypocotyl cell elongation to the WT level is in agreement with our idea that other tissue-specific networks are likely involved in hypocotyl growth (e.g., SCR in the endodermis).

We further found that both *scr-5* and *ProSHR::SHR-GFP; shr-2 scr-5* exhibited a short-hypocotyl phenotype, thus indicating that SCR might also be involved in controlling cell elongation in the etiolated hypocotyl. Interestingly, hypocotyl elongation of the etiolated *shr-6* seedling carrying the non-mobile SHR (*ProSHR::SHR-nlsGFP;shr*-6) was similar to that of both *scr-5* and *ProSHR::SHR-GFP;shr-2 scr-5*, indicating that SHR in the stele was insufficient to fully rescue hypocotyl elongation. Therefore, as previously reported (Ubeda-Tomás et al., 2008; Uchida et al., 2012), it is tempting to speculate that intertissue communication between stele and endodermis exists and is necessary for coordinating cell elongation in the etiolated Arabidopsis hypocotyl.

In conclusion, we have uncovered the novel regulatory roles of SHR in the etiolated Arabidopsis hypocotyl (Fig. 6): i) SHR is necessary for cell elongation; ii) SHR, being associated with their promoters, activates the transcription of the three *XTH* genes (*XTH18*, *XTH22* and *XTH24*) in a SCR-independent manner; and iii) the SCR-independent SHR pathway exists and operates in the Arabidopsis hypocotyl stele.

Note: Supplementary information is available on the Molecules and Cells website (www.molcells.org).

ACKNOWLEDGMENTS

We thank Philip Benfey, Kim Gallagher, Ji-Young Lee, Arabidopsis Biological Resource Center (ABRC) and Nottingham Arabidopsis Stock Centre (NASC) for plant lines. We are grateful to Philip Benfey for critical reading and suggestions. This work was supported by the National Research Foundation (NRF-2021R1F1A1063302) and the Next-Generation BioGreen 21 project (SSAC-PJ01316101).

AUTHOR CONTRIBUTIONS

S.D. and J.L. conceived and designed the research plans. S.D. and J.K. performed experiments. E.K.Y. analyzed microarray and RNA-Seq data. S.J. and K.K. performed plant work including genotyping. S.D., J.K., and J.L. wrote the manuscript with contributions of all the authors. All authors have seen and approved the manuscript in final form prior to submission.

CONFLICT OF INTEREST

The authors have no potential conflicts of interest to disclose.

ORCID

Souvik Dhar https://orcid.org/0000-0002-9693-8145
Jinkwon Kim https://orcid.org/0000-0002-2979-0427
Eun Kyung Yoon https://orcid.org/0000-0001-8690-7989
Sejeong Jang https://orcid.org/0000-0001-6106-9579

Kangseok Ko https://orcid.org/0000-0002-3074-6917
Jun Lim https://orcid.org/0000-0002-0237-3463

REFERENCES

Bai, M.Y., Shang, J.X., Oh, E., Fan, M., Bai, Y., Zentella, R., Sun, T.P., and Wang, Z.Y. (2012). Brassinosteroid, gibberellin and phytochrome impinge on a common transcription module in Arabidopsis. Nat. Cell Biol. *14*, 810-817.

Beemster, G.T. and Baskin, T.I. (1998). Analysis of cell division and elongation underlying the developmental acceleration of root growth in *Arabidopsis thaliana*. Plant Physiol. *116*, 1515-1526.

Benfey, P.N., Linstead, P.J., Roberts, K., Schiefelbein, J.W., Hauser, M.T., and Aeschbacher, R.A. (1993). Root development in Arabidopsis: four mutants with dramatically altered root morphogenesis. Development *119*, 57-70.

Bolger, A.M., Lohse, M., and Usadel, B. (2014). Trimmomatic: a flexible trimmer for Illumina sequence data. Bioinformatics *30*, 2114-2120.

Boron, A.K. and Vissenberg, K. (2014). The *Arabidopsis thaliana* hypocotyl, a model to identify and study control mechanisms of cellular expansion. Plant Cell Rep. *33*, 697-706.

Carlsbecker, A., Lee, J.Y., Roberts, C.J., Dettmer, J., Lehesranta, S., Zhou, J., Lindgren, O., Moreno-Risueno, M.A., Vaten, A., Thitamadee, S., et al. (2010). Cell signalling by microRNA165/6 directs gene dose-dependent root cell fate. Nature *465*, 316-321.

Chaiwanon, J., Wang, W., Zhu, J.Y., Oh, E., and Wang, Z.Y. (2016). Information integration and communication in plant growth regulation. Cell *164*, 1257-1268.

Chebli, Y. and Geitmann, A. (2017). Cellular growth in plants requires regulation of cell wall biochemistry. Curr. Opin. Cell Biol. *44*, 28-35.

Clark, N.M., Hinde, E., Winter, C.M., Fisher, A.P., Crosti, G., Blilou, I., Gratton, E., Benfey, P.N., and Sozzani, R. (2016). Tracking transcription factor mobility and interaction in Arabidopsis roots with fluorescence correlation spectroscopy. Elife *5*, e14770.

Clough, S. and Bent, A. (1998). Floral dip: a simplified method for *Agrobacterium*-mediated transformation of *Arabidopsis thaliana*. Plant J. *16*, 735-743.

Cosgrove, D.J. (2005). Growth of the plant cell wall. Nat. Rev. Mol. Cell Biol. *6*, 850-861.

Cosgrove, D.J. (2016a). Plant cell wall extensibility: connecting plant cell growth with cell wall structure, mechanics, and the action of wall-modifying enzymes. J. Exp. Bot. *67*, 463-476.

Cosgrove, D.J. (2016b). Catalysts of plant cell wall loosening. F1000Res. *5*, F1000 Faculty Rev-119.

Cruz-Ramírez, A., Diaz-Trivino, S., Blilou, I., Grieneisen, V.A., Sozzani, R., Zamioudis, C., Miskolczi, P., Nieuwland, J., Benjamins, R., Dhonukshe, P., et al. (2012). A bistable circuit involving SCARECROW-RETINOBLASTOMA integrates cues to inform asymmetric stem cell division. Cell *150*, 1002-1015.

Cui, H., Hao, Y.L., Kovtun, M., Stolc, V., Deng, X.W., Sakakibara, H., and Kojima, M. (2011). Genome-wide direct target analysis reveals a role for SHORT-ROOT in root vascular patterning through cytokinin homeostasis. Plant Physiol. *157*, 1221-1231.

Cui, H., Levesque, M.P., Vernoux, T., Jung, J.W., Paquette, A.J., Gallagher, K.L., Wang, J.Y., Blilou, I., Scheres, B., and Benfey, P.N. (2007). An evolutionarily conserved mechanism delimiting SHR movement defines a single layer of endodermis in plants. Science *316*, 421-425.

Curtis, M.D. and Grossniklaus, U. (2003). A gateway cloning vector set for high-throughput functional analysis of genes in planta. Plant Physiol. *133*, 462-469.

De Lucas, M., Daviere, J.M., Rodriguez-Falcon, M., Pontin, M., Iglesias-Pedraz, J.M., Lorrain, S., Fankhauser, C., Blazquez, M.A., Titarenko, E., and Prat, S. (2008). A molecular framework for light and gibberellin control of cell elongation. Nature *451*, 480-484.

Dhondt, S., Coppens, F., De Winter, F., Swarup, K., Merks, R.M., Inzé, D., Bennett, M.J., and Beemster, G.T. (2010). SHORT-ROOT and SCARECROW regulate leaf growth in Arabidopsis by stimulating S-phase progression of the cell cycle. Plant Physiol. *154*, 1183-1195.

Di Laurenzio, L., Wysocka-Diller, J., Malamy, J.E., Pysh, L., Helariutta, Y., Freshour, G., Hahn, M.G., Feldmann, K.A., and Benfey, P.N. (1996). The *SCARECROW* gene regulates an asymmetric cell division that is essential for generating the radial organization of the Arabidopsis root. Cell *86*, 423-433.

Earley, K.W., Haag, J.R., Pontes, O., Opper, K., Juehne, T., Song, K., and Pikaard, C.S. (2006). Gateway-compatible vectors for plant functional genomics and proteomics. Plant J. *45*, 616-629.

Eklöf, J.M. and Brumer, H. (2010). The *XTH* gene family: an update on enzyme structure, function, and phylogeny in xyloglucan remodeling. Plant Physiol. *153*, 456-466.

Feng, S., Martinez, C., Gusmaroli, G., Wang, Y., Zhou, J., Wang, F., Chen, L., Yu, L., Iglesias-Pedraz, J.M., Kircher, S., et al. (2008). Coordinated regulation of *Arabidopsis thaliana* development by light and gibberellins. Nature *451*, 475-479.

Fukaki, H., Wysocka-Diller, J., Kato, T., Fujisawa, H., Benfey, P.N., and Tasaka, M. (1998). Genetic evidence that the endodermis is essential for shoot gravitropism in *Arabidopsis thaliana*. Plant J. *14*, 425-430.

Gallagher, K.L. and Benfey, P.N. (2009). Both the conserved GRAS domain and nuclear localization are required for SHORT-ROOT movement. Plant J. *57*, 785-797.

Gallagher, K.L., Paquette, A.J., Nakajima, K., and Benfey, P.N. (2004). Mechanisms regulating SHORT-ROOT intercellular movement. Curr. Biol. *14*, 1847-1851.

Gardiner, J., Donner, T.J., and Scarpella, E. (2011). Simultaneous activation of *SHR* and *ATHB8* expression defines switch to preprocambial cell state in Arabidopsis leaf development. Dev. Dyn. *240*, 261-270.

Gendreau, E., Traas, J., Desnos, T., Grandjean, O., Caboche, M., and Hofte, H. (1997). Cellular basis of hypocotyl growth in *Arabidopsis thaliana*. Plant Physiol. *114,* 295-305.

Helariutta, Y., Fukaki, H., Wysocka-Diller, J., Nakajima, K., Jung, J., Sena, G., Hauser, M.T., and Benfey, P.N. (2000). The *SHORT-ROOT* gene controls radial patterning of the Arabidopsis root through radial signaling. Cell *101*, 555-567.

Heo, J.O., Chang, K.S., Kim, I.A., Lee, M.H., Lee, S.A., Song, S.K., Lee, M.M., and Lim, J. (2011). Funneling of gibberellin signaling by the GRAS transcription regulator SCARECROW-LIKE 3 in the Arabidopsis root. Proc. Natl. Acad. Sci. U. S. A. *108*, 2166-2171.

Hirano, Y., Nakagawa, M., Suyama, T., Murase, K., Shirakawa, M., Takayama, S., Sun, T.P., and Hakoshima, T. (2017). Structure of the SHR–SCR heterodimer bound to the BIRD/IDD transcriptional factor JKD. Nat. Plants *3*, 17010.

Huang, D.W., Sherman, B.T., and Lempicki, R.A. (2009). Systematic and integrative analysis of large gene lists using DAVID bioinformatics resources. Nat. Protoc. *4*, 44-57.

Kim, G., Dhar, S., and Lim, J. (2017). The SHORT-ROOT regulatory network in the endodermis development of Arabidopsis roots and shoots. J. Plant Biol. *60*, 306-313.

Koizumi, K., Hayashi, T., and Gallagher, K.L. (2012a). SCARECROW reinforces SHORT-ROOT signaling and inhibits periclinal cell divisions in the ground tissue by maintaining SHR at high levels in the endodermis. Plant Signal. Behav. *7*, 1573-1577.

Koizumi, K., Hayashi, T., Wu, S., and Gallagher, K.L. (2012b). The SHORT-ROOT protein acts as a mobile, dose-dependent signal in patterning the ground tissue. Proc. Natl. Acad. Sci. U. S. A. *109*, 13010-13015.

Lee, D., Polisensky, D.H., and Braam, J. (2005). Genome-wide identification of touch- and darkness-regulated Arabidopsis genes: a focus on calmodulin-like and *XTH* genes. New Phytol. *165*, 429-444.

Lee, S.A., Jang, S., Yoon, E.K., Heo, J.O., Chang, K.S., Choi, J.W., Dhar, S., Kim, G., Choe, J.E., Heo, J.B., et al. (2016). Interplay between ABA and GA modulates the timing of asymmetric cell divisions in the Arabidopsis root ground tissue. Mol. Plant *9*, 870-884.

Levesque, M.P., Vernoux, T., Busch, W., Cui, H., Wang, J.Y., Blilou, I., Hassan, H., Nakajima, K., Matsumoto, N., Lohmann, J.U., et al. (2006). Whole-genome analysis of the SHORT-ROOT developmental pathway in Arabidopsis. PLoS Biol. *4*, e143.

Lucas, M., Swarup, R., Paponov, I.A., Swarup, K., Casimiro, I., Lake, D., Peret, B., Zappala, S., Mairhofer, S., Whitworth, M., et al. (2011). SHORT-ROOT regulates primary, lateral, and adventitious root development in Arabidopsis. Plant Physiol. *155*, 384-398.

Marsch-Martínez, N., Franken, J., Gonzalez-Aguilera, K.L., de Folter, S., Angenent, G., and Alvarez-Buylla, E.R. (2013). An efficient flat-surface collar-free grafting method for *Arabidopsis thaliana* seedlings. Plant Methods *9*, 14.

Miedes, E., Suslov, D., Vandenbussche, F., Kenobi, K., Ivakov, A., Van Der Straeten, D., Lorences, E.P., Mellerowicz, E.J., Verbelen, J.P., and Vissenberg, K. (2013). Xyloglucan endotransglucosylase/hydrolase (XTH) overexpression affects growth and cell wall mechanics in etiolated Arabidopsis hypocotyls. J. Exp. Bot. *64*, 2481-2497.

Morita, M.T., Saito, C., Nakano, A., and Tasaka, M. (2007). *endodermal-amyloplast less 1* is a novel allele of *SHORT-ROOT*. Adv. Space Res. *39*, 1127-1133.

Nakajima, K., Sena, G., Nawy, T., and Benfey, P.N. (2001). Intercellular movement of the putative transcription factor SHR in root patterning. Nature *413*, 307-311.

Oh, E., Zhu, J.Y., Bai, M.Y., Arenhart, R.A., Sun, Y., and Wang, Z.Y. (2014). Cell elongation is regulated through a central circuit of interacting transcription factors in the Arabidopsis hypocotyl. Elife *3*, e03031.

Paquette, A.J. and Benfey, P.N. (2005). Maturation of the ground tissue of the root is regulated by gibberellin and *SCARECROW* and requires *SHORT-ROOT*. Plant Physiol. *138*, 636-640.

Pysh, L.D., Wysocka-Diller, J.W., Camilleri, C., Bouchez, D., and Benfey, P.N. (1999). The GRAS gene family in Arabidopsis: sequence characterization and basic expression analysis of the *SCARECROW-LIKE* genes. Plant J. *18*, 111-119.

Refrégier, G., Pelletier, S., Jaillard, D., and Höfte, H. (2004). Interaction between wall deposition and cell elongation in dark-grown hypocotyl cells in Arabidopsis. Plant Physiol. *135*, 959-968.

Rose, J.K., Braam, J., Fry, S.C., and Nishitani, K. (2002). The XTH family of enzymes involved in xyloglucan endotransglucosylation and endohydrolysis: current perspectives and a new unifying nomenclature. Plant Cell Physiol. *43*, 1421-1435.

Sablowski, R. (2016). Coordination of plant cell growth and division: collective control or mutual agreement? Curr. Opin. Plant Biol. *34*, 54-60.

Sablowski, R. and Gutierrez, C. (2021). Cycling in a crowd: coordination of plant cell division, growth and cell fate. Plant Cell 2021 Sep 8 [Epub]. https://doi.org/10.1093/plcell/koab222

Sozzani, R., Cui, H., Moreno-Risueno, M., Busch, W., Van Norman, J., Vernoux, T., Brady, S., Dewitte, W., Murray, J., and Benfey, P. (2010). Spatiotemporal regulation of cell-cycle genes by SHORTROOT links patterning and growth. Nature *466*, 128-132.

Sun, N., Wang, J.J., Gao, Z.X., Dong, J., He, H., Terzaghi, W., Wei, N., Deng, X.W., and Chen, H.D. (2016). Arabidopsis SAURs are critical for differential light regulation of the development of various organs. Proc. Natl. Acad. Sci. U. S. A. *113*, 6071-6076.

Ubeda-Tomás, S., Swarup, R., Coates, J., Swarup, K., Laplaze, L., Beemster, G.T., Hedden, P., Bhalerao, R., and Bennett, M.J. (2008). Root growth in Arabidopsis requires gibberellin/DELLA signaling in the endodermis. Nat. Cell Biol. *10*, 625-628.

Uchida, N., Lee, J.S., Horst, R.J., Lai, H.H., Kajita, R., Kakimoto, T., Tasaka, M., and Torii, K.U. (2012). Regulation of inflorescence architecture by intertissue layer ligand-receptor communication between endodermis and phloem. Proc. Natl. Acad. Sci. U. S. A. *109*, 6337-6342.

Wysocka-Diller, J.W., Helariutta, Y., Fukaki, H., Malamy, J.E., and Benfey, P.N. (2000). Molecular analysis of SCARECROW function reveals a radial patterning mechanism common to root and shoot. Development *127*, 595-603.

Yokoyama, R. and Nishitani, K. (2001). A comprehensive expression analysis of all members of a gene family encoding cell-wall enzymes allowed us to predict *cis*-regulatory regions involved in cell-wall construction in specific organs of Arabidopsis. Plant Cell Physiol. *42*, 1025-1033.

Yoo, S.D., Cho, Y.H., and Sheen, J. (2007). Arabidopsis mesophyll protoplasts: a versatile cell system for transient gene expression analysis. Nat. Protoc. *2*, 1565-1572.

Yoon, E.K., Dhar, S., Lee, M.H., Song, J.H., Lee, S.A., Kim, G., Jang, S., Choi, J.W., Choe, J.E., Kim, J.H., et al. (2016). Conservation and diversification of the SHR-SCR-SCL23 regulatory network in the development of the functional endodermis in Arabidopsis shoots. Mol. Plant *9*, 1197-1209.

Yu, N.I., Lee, S.A., Lee, M.H., Heo, J.O., Chang, K.S., and Lim, J. (2010). Characterization of SHORT-ROOT function in the Arabidopsis root vascular system. Mol. Cells *30*, 113-119.